J|A|C|S
ARTICLES
Published on Web 08/08/2002

A Nanoscale Optical Biosensor: Sensitivity and Selectivity of an Approach Based on the Localized Surface Plasmon Resonance Spectroscopy of Triangular Silver Nanoparticles

Amanda J. Haes and Richard P. Van Duyne*

Contribution from the Department of Chemistry, Northwestern University, Evanston, Illinois 60208-3113

Received March 18, 2002

Abstract: Triangular silver nanoparticles (~100 nm wide and 50 nm high) have remarkable optical properties. In particular, the peak extinction wavelength, λ_{max} of their localized surface plasmon resonance (LSPR) spectrum is unexpectedly sensitive to nanoparticle size, shape, and local (~10−30 nm) external dielectric environment. This sensitivity of the LSPR λ_{max} to the nanoenvironment has allowed us to develop a new class of nanoscale affinity biosensors. The essential characteristics and operational principles of these LSPR nanobiosensors will be illustrated using the well-studied biotin−streptavidin system. Exposure of biotin-functionalized Ag nanotriangles to 100 nM streptavidin (SA) caused a 27.0 nm red-shift in the LSPR λ_{max}. The LSPR λ_{max} shift, $\Delta R/\Delta R_{max}$, versus [SA] response curve was measured over the concentration range 10^{-15} M < [SA] < 10^{-6} M. Comparison of the data with the theoretical normalized response expected for 1:1 binding of a ligand to a multivalent receptor with different sites but invariant affinities yielded approximate values for the saturation response, $\Delta R_{max} = 26.5$ nm, and the surface-confined thermodynamic binding constant $K_{a,surf} = 10^{11}$ M^{-1}. At present, the limit of detection (LOD) for the LSPR nanobiosensor is found to be in the low-picomolar to high-femtomolar region. A strategy to amplify the response of the LSPR nanobiosensor using biotinylated Au colloids and thereby further improve the LOD is demonstrated. Several control experiments were performed to define the LSPR nanobiosensor's response to nonspecific binding as well as to demonstrate its response to the specific binding of another protein. These include the following: (1) electrostatic binding of SA to a nonbiotinylated surface, (2) nonspecific interactions of prebiotinylated SA to a biotinylated surface, (3) nonspecific interactions of bovine serum albumin to a biotinylated surface, and (4) specific binding of anti-biotin to a biotinylated surface. The LSPR nanobiosensor provides a pathway to ultrasensitive biodetection experiments with extremely simple, small, light, robust, low-cost instrumentation that will greatly facilitate field-portable environmental or point-of-service medical diagnostic applications.

Introduction

The development of biosensors for the diagnosis and monitoring of diseases, drug discovery, proteomics, and environmental detection of biological agents is an extremely significant problem.[1] Fundamentally, a biosensor is derived from the coupling of a ligand−receptor binding reaction[2] to a signal transducer. Much biosensor research has been devoted to the evaluation of the relative merits of various signal transduction methods including optical,[3,4] radioactive,[5,6] electrochemical,[7,8] piezoelectric,[9,10] magnetic,[11,12] micromechanical,[13,14] and mass spectrometric.[15,16] Although each of these methods has its individual strengths and weaknesses, a strong case has been made that optical sensors, in particular those based on evanescent electromagnetic fields such as propagating surface plasmon polaritons (SPP) at planar gold surfaces, are fast becoming the methods of choice in many affinity biosensing applications.[4,17]

SPP, or more commonly, surface plasmon resonance (SPR) spectroscopy has been widely used to monitor a broad range of

* To whom correspondence should be addressed. E-mail: vanduyne@chem.northwestern.edu.

(1) Turner, A. P. F. *Science* **2000**, *290*, 1315−1317.
(2) Klotz, I. M. *Ligand−Receptor Energetics: A Guide for the Perplexed*; Wiley: New York, 1997.
(3) Lee, H. J.; Goodrich, T. T.; Corn, R. M. *Anal. Chem.* **2001**, *73*, 5525−5531.
(4) Hall, D. *Anal. Biochem.* **2001**, *288*, 109−125.
(5) Wang, J.; Cai, X.; Rivas, G.; Shiraishi, H.; Farias, P. A. M.; Dontha, N. *Anal. Chem.* **1996**, *68*, 2629−2634.
(6) Walterbeek, H. T.; van der Meer, A. J. G. M. *J. Environ. Radioact.* **1996**, *33*, 237−254.
(7) Thevenot, D. R.; Toth, K.; Durst, R. A.; Wilson, G. S. *Biosens. Bioelectron.* **2001**, *16*, 121−131.
(8) Mascini, M.; Palchetti, I.; Marrazza, G. *Fresenius' J. Anal. Chem.* **2001**, *369*, 15−22.
(9) Horacek, J.; Skladal, P. *Anal. Chim. Acta* **1997**, *347*, 43−50.
(10) Ebersole, R. C.; Miller, J. A.; Moran, J. R.; Ward, M. D. *J. Am. Chem. Soc.* **1990**, *112*, 3239−3241.
(11) Miller, M. M.; Sheehan, P. E.; Edelstein, R. L.; Tamanaha, C. R.; Zhong, L.; Bounnak, S.; Whitman, L. J.; Colton, R. J. *J. Magn. Magn. Mater.* **2001**, *225*, 156−160.
(12) Chemla, Y. R.; Grossman, H. L.; Poon, Y.; McDermott, R.; Stevens, R.; Alper, M. D.; Clarke, J. *Proc. Natl. Acad Sci. U.S.A.* **2000**, *97*, 26.
(13) Raiteri, R.; Grattarola, M.; Butt, H.-J.; Skladal, P. *Sens. Actuators, B* **2001**, *B79*, 115−126.
(14) Kasemo, B. *Curr. Opin. Solid State Mater. Sci.* **1998**, *3*, 451−459.
(15) Natsume, T.; Nakayama, H.; Isobe, T. *Trends Biotechnol.* **2001**, *19*, S28−S33.
(16) Polla, D. L.; Erdman, A. G.; Robbins, W. P.; Markus, D. T.; Diaz-Diaz, J.; Rizq, R.; Nam, Y.; Brickner, H. T.; Wang, A.; Krulevitch, P. *Annu. Rev. Biomed. Eng.* **2000**, *2*, 551−576.

10.1021/ja020393x CCC: $22.00

analyte−surface binding interactions including the adsorption of small molecules,[18−20] ligand−receptor binding,[21−24] protein adsorption on self-assembled monolayers,[25−27] antibody−antigen binding,[28] DNA and RNA hybridization,[29−32] and protein−DNA interactions.[33] The sensing mechanism of SPR spectroscopy is based on the measurement of small changes in refractive index that occur in response to analyte binding at or near the surface of a noble metal (Au, Ag, Cu) thin film.[34] Chemosensors and biosensors based on SPR spectroscopy possess many desirable characteristics including the following: (1) a refractive index sensitivity on the order of 1 part in 10^5-10^6 corresponding to an areal mass sensitivity of $\sim 10-1$ pg/mm^2;[4,18,19,21] (2) a long-range sensing length scale determined by the exponential decay of the evanescent electromagnetic field, $L_z \sim 200$ nm;[18] (3) multiple instrumental modes of detection (viz., angle shift, wavelength shift, and imaging);[34] (4) real-time detection on the $10^{-1}-10^3$ s time scale for measurement of binding kinetics;[17,19,20,35] and (5) lateral spatial resolution on the order of 10 μm enabling multiplexing and miniaturization especially using the SPR imaging mode of detection.[34] Although SPR spectroscopy is a totally nonselective sensor platform, a high degree of analyte selectivity can be conferred using the specificity of surface-attached ligands and passivation of the sensor surface to nonspecific binding.[4,17,34,36,37] In addition, it is label-free;[36] capable of probing complex mixtures, such as clinical material, without prior purification;[4,34,36] and benefits from the availability of commercial instrumentation with advanced microfluidic sample handling.[38,39]

The development of large-scale biosensor arrays composed of highly miniaturized signal transducer elements that enable the real-time, parallel monitoring of multiple species is an important driving force in biosensor research. This is particularly significant in high-throughput screening applications such as drug discovery and proteomics research where many thousands of ligand−receptor or protein−protein interactions must be rapidly examined. In these situations, it is necessary to utilize sensor platforms that have as many of the desirable characteristics of SPR spectroscopy as possible, but also can be easily configured in array formats and minimize the number of target analyte molecules per sensor element, the time required to achieve measurable signals, and the volume of sample required.

These stringent requirements for high-throughput screening applications present at least three fundamental challenges to SPR spectroscopy. First, the SPR angle and wavelength shift detection modes, which have been multiplexed in small arrays, are cumbersome to implement in very large arrays due to the optical complexity of the instrumentation.[28,38,40] Second, while SPR imaging is an important approach to overcoming this problem, it is limited to signal transducer element sizes of a few square micrometers, more typically 10 μm $\times$ 10 μm, by the excitation wavelength-dependent, lateral propagation length, l_d, of the SPP.[34] Third, real-time sensing or kinetic measurements using SPR spectroscopy are severely mass transport limited by diffusion to time scales on the order of 10^3-10^4 s for analytes at bulk concentrations, $C_{bulk} < 10^{-6}-10^{-7}$ M. Furthermore, since the time required for the analyte surface excess to reach half-saturation coverage scales as the inverse square of C_{bulk},[21] the mass transport problem is greatly exacerbated for C_{bulk} in the low-picomolar or high-femtomolar domains demanded by many bioassays.

Recently, several research groups have begun to explore alternative strategies for the development of optical biosensors[41−59] and chemosensors[41,60−65] based on the extraordinary optical properties of noble metal nanoparticles. Noble metal nanopar-

(17) Schuck, P. *Annu. Rev. Biophys. Biomol. Struct.* **1997**, *26*, 541−566.
(18) Jung, L. S.; Campbell, C. T.; Chinowsky, T. M.; Mar, M. N.; Yee, S. S. *Langmuir* **1998**, *14*, 5636−5648.
(19) Jung, L. S.; Campbell, C. T. *J. Phys. Chem. B* **2000**, *104*, 11168−11178.
(20) Jung, L. S.; Campbell, C. T. *Phys. Rev. Lett.* **2000**, *84*, 5164−5167.
(21) Jung, L. S.; Nelson, K. E.; Stayton, P. S.; Campbell, C. T. *Langmuir* **2000**, *16*, 9421−9432.
(22) Perez-Luna, V. H.; O'Brien, M. J.; Opperman, K. A.; Hampton, P. D.; Lopez, G. P.; Klumb, L. A.; Stayton, P. S. *J. Am. Chem. Soc.* **1999**, *121*, 6469−6478.
(23) Mann, D. A.; Kanai, M.; Maly, D. J.; Kiessling, L. L. *J. Am. Chem. Soc.* **1998**, *120*, 10575−10582.
(24) Hendrix, M.; Priestley, E. S.; Joyce, G. F.; Wong, C.-H. *J. Am. Chem. Soc.* **1997**, *119*, 3641−3648.
(25) Frey, B. L.; Jordan, C. E.; Kornguth, S.; Corn, R. M. *Anal. Chem.* **1995**, *67*, 4482−4457.
(26) Mrksick, M.; Grunwell, J. R.; Whitesides, G. M. *J. Am. Chem. Soc.* **1995**, *117*, 12009−12010.
(27) Rao, J.; Yan, L.; Xu, B.; Whitesides, G. M. *J. Am. Chem. Soc.* **1999**, *121*, 2629−2630.
(28) Berger, C. E. H.; Beumer, T. A. M.; Kooyman, R. P. H.; Greve, J. *Anal. Chem.* **1998**, *70*, 703−706.
(29) Heaton, R. J.; Peterson, A. W.; Georgiadis, R. M. *Proc. Natl. Acad. Sci. U.S.A.* **2001**, *98*, 3701−3704.
(30) Georgiadis, R.; Peterlinz, K. P.; Peterson, A. W. *J. Am. Chem. Soc.* **2000**, *122*, 7837−3173.
(31) Jordan, C. E.; Frutos, A. G.; Thiel, A. J.; Corn, R. M. *Anal. Chem.* **1997**, *69*, 4939−4947.
(32) Nelson, B. P.; Grimsrud, T. E.; Liles, M. R.; Goodman, R. M. *Anal. Chem.* **2001**, *73*, 1−7.
(33) Brockman, J. M.; Frutos, A. G.; Corn, R. M. *J. Am. Chem. Soc.* **1999**, *121*, 8044−8051.
(34) Brockman, J. M.; Nelson, B. P.; Corn, R. M. *Annu. Rev. Phys. Chem.* **2000**, *51*, 41−63.
(35) Knoll, W. *Annu. Rev. Phys. Chem.* **1998**, *49*, 569−638.
(36) Haake, H.-M.; Schutz, A.; Gauglitz, G. *Fresenius' J. Anal. Chem.* **2000**, *366*, 576−585.
(37) Garland, P. B. *Q. Rev. Biophys.* **1996**, *29*, 91−117.
(38) Karlsson, R.; Stahlberg, R. *Anal. Biochem.* **1995**, *228*, 274−280.
(39) Sjolander, S.; Urbaniczky, C. *Anal. Chem.* **1991**, *63*, 2338−2345.
(40) Zizlsperger, M.; Knoll, W. *Prog. Colloid Polym. Sci.* **1998**, *109*, 244−253.
(41) Malinsky, M. D.; Kelly, K. L.; Schatz, G. C.; Van Duyne, R. P. *J. Am. Chem. Soc.* **2001**, *123*, 1471−1482.
(42) Nath, N.; Chilkoti, A. *Anal. Chem.* **2002**, *74*, 504−509.
(43) Connolly, S.; Cobbe, S.; Fitzmaurice, D. *J. Phys. Chem. B* **2001**, *105*, 2222−2226.
(44) Cao, Y. W.; Jin, R.; Mirkin, C. A. *J. Am. Chem. Soc.* **2001**, *123*, 7961−7962.
(45) Englebienne, P.; Van Hoonacker, A.; Verhas, M. *Analyst* **2001**, *126*, 1645−1651.
(46) Eck, D.; Helm, C. A.; Wagner, N. J.; Vaynberg, K. A. *Langmuir* **2001**, *17*, 957−960.
(47) Haynes, C. L.; Van Duyne, R. P. *J. Phys. Chem. B* **2001**, *105*, 5599−5611.
(48) Taton, T. A.; Lu, G.; Mirkin, C. A. *J. Am. Chem. Soc.* **2001**, *123*, 5164−5165.
(49) Storhoff, J. J.; Lazarides, A. A.; Mucic, R. C.; Mirkin, C. A.; Letsinger, R. L.; Schatz, G. C. *J. Am. Chem. Soc.* **2000**, *122*, 4640−4650.
(50) Connolly, S.; Rao, S. N.; Fitzmaurice, D. *J. Am. Chem. Soc.* **2000**, *104*, 4765−4776.
(51) Okamoto, T.; Yamaguchi, I.; Kobayashi, T. *Opt. Lett.* **2000**, *25*, 372−374.
(52) Himmelhaus, M.; Takei, H. *Sens. Actuators, B* **2000**, *B63*, 24−30.
(53) Bauer, G.; Pittner, F.; Schalkhammer, T. *Mikrochim. Acta* **1999**, *131*, 107−114.
(54) Takei, H. *Proc. SPIE-Int. Soc. Opt. Eng.* **1998**, *3515*, 278−283.
(55) Englebienne, P. *Analyst* **1998**, *123*, 1599−1603.
(56) Steiner, G.; Pham, M. T.; Kuhne, C.; Salzer, R. *Fresenius' J. Anal. Chem.* **1998**, *362*, 9−14.
(57) Storhoff, J. J.; Elghanian, R.; Mucic, R. C.; Mirkin, C. A.; Letsinger, R. L. *J. Am. Chem. Soc.* **1998**, *120*, 1959−1964.
(58) Elghanian, R.; Storhoff, J. J.; Mucic, R. C.; Letsinger, R. L.; Mirkin, C. A. *Science* **1997**, *227*, 1078−1080.
(59) Mirkin, C. A.; Letsinger, R. L.; Mucic, R. C.; Storhoff, J. J. *Nature* **1996**, *382*, 607−609.
(60) Kalyuzhny, G.; Schneeweiss, M. A.; Shanzer, A.; Vaskevich, A.; Rubinstein, I. *J. Am. Chem. Soc.* **2001**, *123*, 3177−3178.
(61) Hilger, A.; Cuppers, N.; Tenfelde, M.; Kreibig, U. *Eur. Phys. J. D* **2000**, *10*, 115−118.
(62) Kalyuzhny, G.; Vaskevick, A.; Ashkenasy, G.; Shanzer, A. *J. Phys. Chem. B* **2000**, *104*, 8238−8244.
(63) Sanekata, M.; Suzuka, I. *Chem. Phys, Lett.* **2000**, *323*, 98−104.
(64) Henglein, A.; Meisel, D. *J. Phys. Chem. B* **1998**, *102*, 8364−8366.
(65) Kreibig, U.; Gartz, M.; Hilger, A. *Ber. Bunsen.-Ges.* **1997**, *101*, 1593−1604.

ticles exhibit a strong UV−vis absorption band that is not present in the spectrum of the bulk metal.[47,65−72] This absorption band results when the incident photon frequency is resonant with the collective oscillation of the conduction electrons and is known as the localized surface plasmon resonance (LSPR). LSPR excitation results in wavelength selective absorption with extremely large molar extinction coefficients $\sim 3 \times 10^{11}$ M^{-1} cm^{-1},[73] resonant Rayleigh scattering[74,75] with an efficiency equivalent to that of 10^6 fluorophors,[76,77] and the enhanced local electromagnetic fields near the surface of the nanoparticle which are responsible for the intense signals observed in all surface-enhanced spectroscopies.[78] It is well established that the peak extinction wavelength, λ_{max}, of the LSPR spectrum is dependent upon the size, shape, and interparticle spacing of the nanoparticle as well as its dielectric properties and those of the local environment.[47,65−72] Consequently, there are at least four different nanoparticle-based sensing mechanisms that enable the transduction of macromolecular or chemical binding events into optical signals based on changes in the LSPR extinction or scattering intensity, shifts in LSPR λ_{max}, or both. These mechanisms are: (1) resonant Rayleigh scattering from nanoparticle labels in a manner analogous to fluorescent dye labels,[48,75−77,79−82] (2) nanoparticle aggregation,[43,49,50,57−59] (3) charge-transfer interactions at nanoparticle surfaces,[41,61,64,65,83,84] and (4) local refractive index changes.[41,42,46,51,52,54]

Recently, we demonstrated that nanoscale chemosensors and biosensors can be realized through shifts in the LSPR λ_{max} of triangular silver nanoparticles.[41] These wavelength shifts are caused by adsorbate-induced local refractive index changes in competition with charge-transfer interactions at the nanoparticle surface. Triangular silver nanoparticles have been shown to be unexpectedly sensitive to nanoparticle size, shape, and local dielectric environment.[41,47,73,85,86] Systematic studies established that the LSPR λ_{max} of triangular Ag nanoparticles was so sensitive to the presence of alkanethiol adsorbates that it exhibited a linear red-shift corresponding to 3.0 nm for every carbon atom in the alkane chain accompanied by an 8.5 nm blue-shift due to the Ag−S charge-transfer interaction.[41] Furthermore, it should be noted that these LSPR wavelength shifts are caused by only 60 000 alkanethiol molecules/nanoparticle. As an additional proof of concept, it was shown that the LSPR λ_{max} reversibly red-shifted by ~5 nm in response to the electrostatic adsorption of the polypeptide poly-(L)-lysine (PL) to Ag nanoparticles modified with deprotonated carboxylate groups from 11-mercaptoundecanoic acid (11-MUA).

In this paper, a detailed study is presented demonstrating that triangular silver nanoparticles fabricated by nanosphere lithography (NSL)[47] function as extremely sensitive and selective nanoscale affinity biosensors. It will be shown that these nanoscale biosensors based on LSPR spectroscopy operate in a manner totally analogous to their SPR counterparts by transducing small changes in refractive index near the noble metal surface into a measurable wavelength shift response. The well-studied biotin−streptavidin (SA) system with its extremely high binding affinity ($K_a \sim 10^{13}$ M^{-1}) is chosen to illustrate the attributes of these LSPR-based nanoscale affinity biosensors.[87] The biotin−SA system has been studied in great detail by SPR spectroscopy[21,22] and serves as an excellent model system for the LSPR nanosensor. SA, a tetrameric protein, can bind up to four biotinylated molecules (i.e., antibodies, inhibitors, nucleic acids, etc.) with minimal impact on its biological activity and, therefore, will provide a ready pathway for extending the analyte accessibility of the LSPR nanobiosensor.[88] The LSPR λ_{max} shift, $\Delta R/\Delta R_{max}$, versus [SA] response curve was measured over the concentration range 10^{-15} M < [SA] < 10^{-6} M. Comparison of the data with theoretical expectations yielded a saturation response, $\Delta R_{max} = 26.5$ nm, surface-confined thermodynamic binding constant $K_{a,surf} = 10^{11}$ M^{-1} and limit of detection (LOD) in the low-picomolar to high-femtomolar region. Amplification of the LSPR nanobiosensor response is demonstrated using biotinylated Au colloids. We anticipate that further improvements in the LOD will be achieved soon.

Additionally, we will demonstrate that LSPR nanosensors possess at least two unique characteristics based on nanoparticle size and shape including the following: (1) refractive index sensitivity on the order of 1 part in 10^2 that, nevertheless, corresponds to an areal mass sensitivity of ~100−1000 pg/mm^2 and (2) short-range, sensing length scale determined by the characteristic decay length of the local electromagnetic field, $L_z \sim 5-6$ nm. Furthermore, LSPR nanosensors retain the high selectivity, label-free operation, capability to probe complex mixtures without purification and multiple detection modes (viz., extinction and resonance Rayleigh scattering) characteristic of or analogous to sensors based on SPR spectroscopy. From the instrumentation perspective, LSPR nanosensors can be implemented using extremely simple, small, light, robust, low-cost equipment for unpolarized, UV−visible extinction spectroscopy in transmission or reflection geometry. The instrumental simplicity of the LSPR nanosensor approach is expected to greatly facilitate field-portable environmental or point-of-service medical diagnostic applications.

(66) Mulvaney, P. *MRS Bull.* **2001**, *26*, 1009−1014.
(67) El-Sayed, M. A. *Acc. Chem. Res.* **2001**, *34*, 257−264.
(68) Link, S.; El-Sayed, M. A. *J. Phys. Chem. B* **1999**, *103*, 8410−8426.
(69) Kreibig, U.; Gartz, M.; Hilger, A.; Hovel, H. In *Cluster Materials*; Duncan, M. A., Ed.; Advances in Metal and Semiconductor Clusters 4; JAI Press Inc.: Stamford, CT, 1998; pp 345−393.
(70) Mulvaney, P. *Langmuir* **1996**, *12*, 788−800.
(71) Kreibig, U. In *Handbook of Optical Properties*; Hummel, R. E., Wissmann, P., Eds.; CRC Press: Boca Raton, FL, 1997; Vol. II, pp 145−190.
(72) Jensen, T. R.; Kelly, K. L.; Lazarides, A.; Schatz, G. C. *J. Cluster Sci.* **1999**, *10*, 295−317.
(73) Jensen, T. R.; Malinsky, M. D.; Haynes, C. L.; Van Duyne, R. P. *J. Phys. Chem. B* **2000**, *104*, 10549−10556.
(74) Michaels, A. M.; Nirmal, M.; Brus, L. E. *J. Am. Chem. Soc.* **1999**, *121*, 9932−9939.
(75) Schultz, S.; Smith, D. R.; Mock, J. J.; Schultz, D. A. *Proc. Natl. Acad. Sci. U.S.A.* **2000**, *97*, 996−1001.
(76) Yguerabide, J.; Yguerabide, E. E. *Anal. Biochem.* **1998**, *262*, 137−156.
(77) Yguerabide, J.; Yguerabide, E. E. *Anal. Biochem.* **1998**, *262*, 157−176.
(78) Schatz, G. C.; Van Duyne, R. P. In *Handbook of Vibrational Spectroscopy*; Chalmers, J. M., Griffiths, P. R., Eds.; Wiley: New York, 2002; Vol. 1, pp 759−774.
(79) Taton, T. A.; Mirkin, C. A.; Letsinger, R. L. *Science* **2000**, *289*, 1757−1760.
(80) Sonnichsen, C.; Geier, S.; Hecker, N. E.; von Plessen, G.; Feldmann, J.; Ditlbacher, H.; Lamprecht, B.; Krenn, J. R.; Aussenegg, F. R.; Chan, V. Z.-H.; Spatz, J. P.; Moller, M. *Appl. Phys. Lett.* **2000**, *77*, 2949−2951.
(81) Sonnichsen, C.; Franzl, T.; Wilk, T.; von Plessen, G.; Feldmann, J.; Wilson, O.; Mulvaney, P. *Phys. Rev. Lett.* **2002**, *88*, 077402/077401−077401−077402/077404.
(82) Bao, P.; Frutos, A. G.; Greef, C.; Lahiri, J.; Muller, U.; Peterson, T. C.; Wardern, L.; Xie, X. *Anal. Chem.* **2002**, *74*, 1792−1297.
(83) Kreibig, U.; Vollmer, M. *Optical Properties of Metal Clusters*; Springer-Verlag: Heidelberg, Germany, 1995; Vol. 25.
(84) Linnert, T.; Mulvaney, P.; Henglein, A. *J. Phys. Chem.* **1993**, *97*, 679−682.
(85) Jin, R.; Cao, Y. W.; Mirkin, C. A.; Kelly, K. L.; Schatz, G. C.; Zheng, J. G. *Science* **2001**, *294*, 1901−1903.
(86) Jensen, T. R.; Schatz, G. C.; Van Duyne, R. P. *J. Phys. Chem. B* **1999**, *103*, 2394−2401.
(87) Green, N. M. *Adv. Protein Chem.* **1975**, *29*, 85−133.
(88) Wilchek, M.; Bayer, E. A. In *Avidin−Biotin Immobilization Systems*; Cass, T., Ligler, F. S., Eds.; Oxford University Press: Oxford, U.K., 1998; pp 15−34.

We anticipate that future improvements in these size and shape tunable nanosensor materials, when coupled with recently developed single-nanoparticle spectroscopic techniques,[80] will (1) reduce the time scale for real-time detection and the study of protein binding kinetics by 2−3 orders of magnitude and (2) improve the lateral spatial resolution to the single-nanoparticle limit. These attributes, if experimentally realized, should enable massively parallel bioassays, dramatically reduce mass transport limitation, and approach sensitivities of a few molecules, perhaps even a single molecule, per nanoparticle.

Experimental and Methods

Materials. 11-Mercaptoundecanoic acid, 1-octanethiol (1-OT), $HAuCl_4$, $[CH_3(CH_2)_7]_4NBr$, $NaBH_4$, hexanes, and methanol were acquired from Aldrich (Milwaukee, WI). Anti-biotin, 1-ethyl-3-[3-dimethylaminopropyl]carbodiimide hydrochloride (EDC), bovine serum albumin (BSA), streptavidin, and 10 and 20 mM phosphate-buffered saline (PBS), pH = 7.4, was obtained from Sigma (St. Louis, MO). (+)-Biotinyl-3,6-dioxaoctanediamine (biotin) was purchased from Pierce (Rockford, IL). Absolute ethanol was purchased from Pharmco (Brookfield, CT). Ag wire (99.99%, 0.5 mm diameter) was obtained from D. F. Goldsmith (Evanston, IL). Borosilicate glass substrates, Fisherbrand No. 2 18 mm circle coverslips were purchased from Fisher Scientific (Pittsburgh, PA). Tungsten vapor deposition boats were acquired from R. D. Mathis (Long Beach, CA). Polystyrene nanospheres with diameters of 400 ± 7 nm were received as a suspension in water (Interfacial Dynamics Corp., Portland, OR) and were used without further treatment. Millipore cartridges (Marlborough, MA) were used to purify water to a resistivity of 18 MΩ. All materials were used without further purification.

Biotinylated Au Colloid Preparation. Au colloids were first functionalized with carboxylic acid terminal groups.[89,90] $HAuCl_4$ (0.596 g) was added to 57 mL of water. $[CH_3(CH_2)_7]_4NBr$ (1.046 g) in chloroform (45 mL) was then added to the Au solution and stirred for 10 min. The chloroform layer was separated and mixed with 11-MUA (0.022 g) and 1-OT (0.044 g, 15 mL of chloroform). $NaBH_4$ (0.450 g, 51 mL of H_2O) was added slowly and was allowed to stir for 12 h. The functionalized Au colloids were centrifuged out of solution, dried under N_2, and resuspended in H_2O. Next, EDC (0.019 g) and biotin (0.054 g) were added to 3 mL of Au colloids (4.5×10^{13} particles/L) and allowed to react for 24 h. The resulting colloids had diameters ranging from 10 to 20 nm.

Substrate Preparation. Glass substrates were cleaned in a piranha solution (1:3 30% H_2O_2/H_2SO_4) at 80 °C for 30 min. Once cooled, the glass substrates were rinsed with copious amounts of water and then sonicated for 60 min in 5:1:1 $H_2O/NH_4OH/30\%$ H_2O_2. Next, the glass was rinsed repeatedly with water and was stored in water until used.

Nanoparticle Preparation. NSL was used to fabricate monodisperse, surface-confined Ag nanoparticles.[47] For these experiments, single-layer colloidal crystal nanosphere masks were prepared by drop coating ~2 μL of nanosphere solution onto glass substrates. Once the nanosphere masks were dry, the substrates were mounted into a Consolidated Vacuum Corp. vapor deposition system. A Leybold Inficon XTM/2 quartz crystal microbalance (East Syracuse, NY) was used to measure the thickness of the Ag film deposited over the nanosphere mask. Ag films were deposited to 50.0 nm thicknesses for all samples in this study. Following Ag deposition, the nanosphere mask was removed by sonicating the sample in ethanol for 3 min.

Ultraviolet−Visible Extinction Spectroscopy. Macroscale UV−visible extinction measurements were collected using an Ocean Optics (Dunedin, FL) SD2000 fiber optically coupled spectrometer with a CCD detector. All spectra collected are macroscopic measurements performed in standard transmission geometry with unpolarized light. The probe beam diameter was ~4 mm.

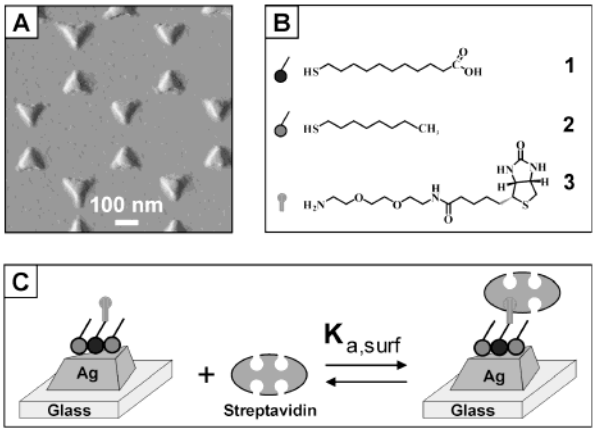

Figure 1. LSPR Nanobiosensor. (A) Tapping mode AFM image of the Ag nanoparticles (nanosphere diameter, D = 400 nm; mass thickness, d_m = 50.0 nm Ag on a glass substrate). Scan area, 1.0 μm^2. Scan rate between 1 and 2 Hz. After solvent annealing, the resulting nanoparticles have in-plane widths of ~100 nm and out-of-plane heights of ~51 nm. (B) Surface chemistry of the Ag nanobiosensor. A mixed monolayer of (1) 11-MUA and (2) 1-OT is formed on the exposed surfaces of the Ag nanoparticles followed by the covalent linking of (3) biotin to the carboxyl groups of (1) 11-MUA. (C) Schematic representation of SA binding to a biotinylated Ag nanobiosensor fabricated by NSL on a glass substrate.

Nanoparticle Annealing. A home-built flow cell[41] was used to control the external environment of the Ag nanoparticle substrates. Prior to modification, the Ag nanoparticles were solvent annealed[41] with hexanes and methanol. Dry N_2 gas and solvent were cycled through the flow cell until the λ_{max} of the sample stabilized. Samples were then incubated in 1 mM 3:1 1-OT/11-MUA ethanolic solutions for 24 h. After incubation, the nanoparticle samples were rinsed with ethanol and dried by flowing N_2 gas through the sample cell. Next, 1 mM biotin in 10 mM PBS was covalently linked to the surface carboxyl groups using EDC coupling over a 3-h period. Following thorough rinsing and N_2 drying, the samples were incubated in SA solutions in 10 mM PBS for 3 h. Samples were rinsed thoroughly with 10 mM PBS, 20 mM PBS, and water to remove electrostatically bound molecules.

Atomic Force Microscopy (AFM). AFM images were collected using a Digital Instruments Nanoscope III microscope operating in tapping mode. Etched Si nanoprobe tips (TESP, Digital Instruments, Santa Barbara, CA) were used. These tips had resonance frequencies between 280 and 320 kHz and are conical in shape with a cone angle of 20° and an effective radius of curvature at the tip of 10 nm. All images shown here are unfiltered data that were collected in ambient conditions.

Results and Discussion

Fabrication and Surface Modification of the LSPR Nanobiosensor. NSL was used to create surface-confined triangular Ag nanoparticles supported on a glass substrate (Figure 1A). The Ag nanotriangles have in-plane widths of ~100 nm and out-of-plane heights of ~51 nm as determined by AFM. To prepare the LSPR nanosensor for biosensing events, the Ag nanotriangles are first functionalized with a self-assembled monolayer (SAM) composed of 3:1 1-OT (Figure 1B-2)/11-MUA (Figure 1B-1) resulting in a surface coverage corresponding to 0.1 monolayer of carboxylate binding sites.[91] Since the maximum number of alkanethiol molecules per nanoparticle is 60 000, this is equivalent to ~6000 carboxylate binding sites/nanoparticle. Next, biotin (Figure 1B-3) was covalently attached

(89) Weisbecker, C. S.; Merritt, M. V.; Whitesides, G. M. *Langmuir* **1996**, *12*, 3763−3772.
(90) Matsui, H.; Pan, S.; Douberly, G. E. *J. Phys. Chem. B* **2001**, *105*, 1683−1686.

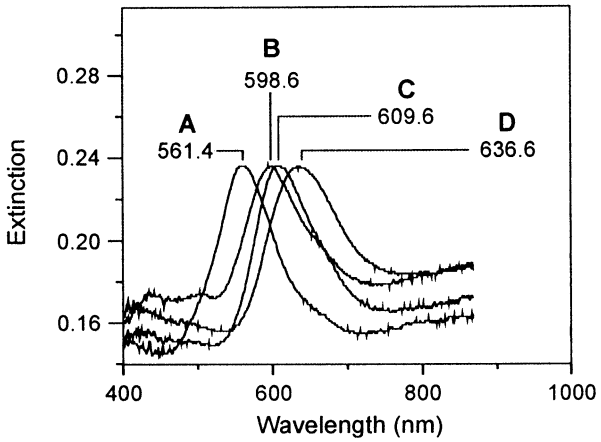

Figure 2. LSPR spectra of each step in the surface modification of NSL-derived Ag nanoparticles to form a biotinylated Ag nanobiosensor and the specific binding of SA. (A) Ag nanoparticles before chemical modification, $\lambda_{max} = 561.4$ nm. (B) Ag nanoparticles after modification with 1 mM 1:3 11-MUA/1-OT, $\lambda_{max} = 598.6$ nm. (C) Ag nanoparticles after modification with 1 mM biotin, $\lambda_{max} = 609.6$ nm. (D) Ag nanoparticles after modification with 100 nM SA, $\lambda_{max} = 636.6$ nm. All extinction measurements were collected in a N_2 environment.

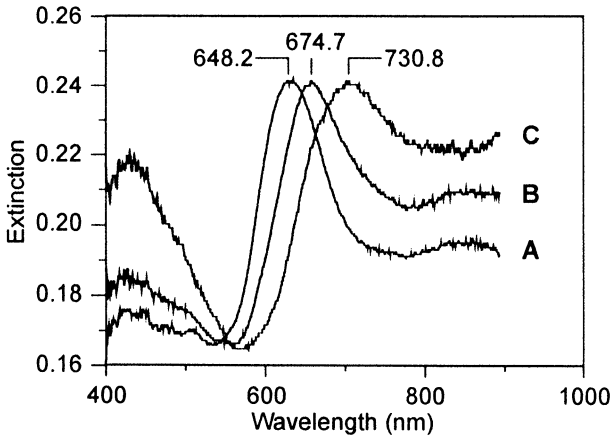

Figure 3. LSPR spectra illustrating the amplification of the saturation coverage SA response using biotinylated Au colloids. (A) Ag nanoparticles after modification with 1 mM biotin, $\lambda_{max} = 648.2$ nm. (B) Ag nanoparticles after modification with 100 nM SA, $\lambda_{max} = 674.7$ nm. (C) Ag nanoparticles after modification with biotinylated Au colloids, $\lambda_{max} = 730.8$ nm. All spectra were collected in a N_2 environment.

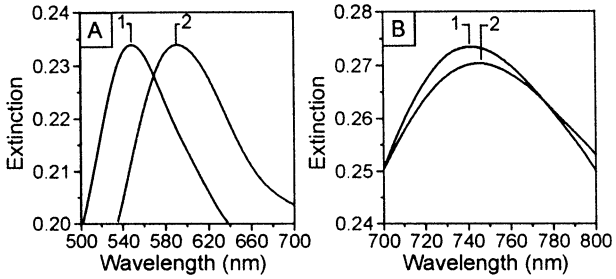

Figure 4. Smoothed LSPR spectra illustrating the response of the Ag nanobiosensor to [SA] corresponding to saturation coverage and limit of detection. All extinction measurements were collected in a N_2 environment. (A) Ag nanoparticles (1) before ($\lambda_{max} = 609.6$ nm) and (2) after ($\lambda_{max} = 636.6$ nm) 100 nM SA exposure. (B) Ag nanoparticles (1) before ($\lambda_{max} = 741.0$ nm) and (2) after ($\lambda_{max} = 744.8$ nm) 1 pM SA exposure.

to the carboxylate groups using EDC. The number of resulting biotin sites will be determined by the yield of the EDC coupling reaction. Since this is likely to be ~1−5% efficient,[92] one expects there to be only 60−300 biotin sites/nanoparticle at maximum coverages. A schematic illustration of the LSPR nanobiosensor depicting its exposure to SA is shown in Figure 1C.

Before surface functionalization, the Ag nanoparticles were exposed to solvent and N_2 as described above. In this study, the λ_{max} of the Ag nanoparticles were monitored during each surface functionalization step (Figure 2). First, the LSPR λ_{max} of the bare Ag nanoparticles was measured to be 561.4 nm (Figure 2A). To ensure a well-ordered SAM on the Ag nanoparticles, the sample was incubated in the thiol solution for 24 h. After careful rinsing and thorough drying with N_2 gas, the LSPR λ_{max} after modification with the mixed SAM (Figure 2B) was measured to be 598.6 nm. The LSPR λ_{max} shift corresponding to this surface functionalization step was a 38 nm red-shift; hereafter, + will signify a red-shift and − a blue-shift, with respect to bare Ag nanoparticles. Next, biotin was covalently attached via amide bond formation with a two-unit poly(ethylene glycol) linker to carboxylated surface sites (Figure 2C). The LSPR λ_{max} after biotin attachment (Figure 2C) was measured to be 609.6 nm, corresponding to an additional +11 nm shift. The LSPR nanosensor has now been prepared for exposure to the target analyte. Exposure to 100 nM SA, resulted in LSPR $\lambda_{max} = 636.6$ nm (Figure 2D), corresponding to an additional +27 nm shift. It should be noted that the signal transduction mechanism in this nanosensor is a reliably measured wavelength shift rather than an intensity change as in many previously reported nanoparticle-based sensors.

Amplification of the LSPR Wavelength Shift Response Using Biotinylated Au Colloids. Additional sensitivity to the SA analyte can be gained using an LSPR adaptation of the classic bioassay "sandwich". The nanosensor substrate was biotinylated as explained previously (Figure 3A) and exposed to SA (Figure 3B) as in Figure 2. The +27.0 nm LSPR shift measured with 100 nM SA was increased by an additional +56 nm after exposure to biotinylated Au colloids (Figure 3C). Given the size of the Au colloids to SA and the stearic hindrance to the vacant "bottom" binding site (of SA), it is likely that the +56 nm shift is a consequence of binding 1 Au nanoparticle/surface-bound SA. Because the LSPR nanosensor operates by detecting refractive index changes within the localized electromagnetic fields surrounding the nanoparticles; as the layer thickness increases, an additional wavelength shift should be measured. Because the Au colloids extend the adsorbate layer thickness (by a factor of 2), an additional wavelength shift of approximately this magnitude is expected. The data in Figure 3 show a factor of 3 enhancement of the LSPR response.

LSPR Wavelength Shift as a Function of SA Concentration. Exposure of the nanosensor surface to 100 nM SA results in a maximum LSPR response of +27 nm corresponding to saturation binding of SA (Figure 4A). Repeating this experiment with exposure of the nanosensor surface to only 1 pM SA results in a marked decrease of the response to a small, but reproducibly detected, +4 nm shift (Figure 4B). It should be noted that the absolute values of λ_{max} corresponding to Figures 4A-1 and B-1 are different because they were collected from different nanosensor samples. Sample-to-sample variations in the initial λ_{max} values have two sources. First, differences in the local dielectric environment of the nanoparticles caused by adsorption

(91) Bain, C. D.; Whitesides, G. M. *J. Am. Chem. Soc.* **1988**, *110*, 6560−6561.
(92) Jensen, T. R.; Duval, M. L.; Kelly, K. L.; Lazarides, A.; Schatz, G. C.; Van Duyne, R. P. *J. Phys. Chem. B* **1999**, *103*, 9846−9853.

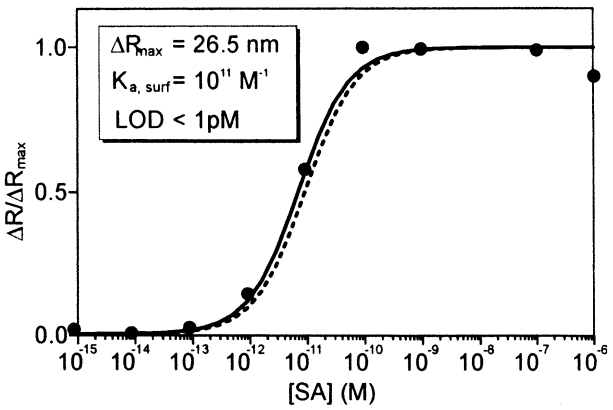

Figure 5. Normalized LSPR shift, $\Delta R/\Delta R_{max}$, versus [SA] response curve for the specific binding of SA to a biotinylated Ag nanobiosensor. The normalized experimental LSPR responses (solid circles) were calculated by subtracting $R_{layer\ 1}$ for the biotinylated Ag nanobiosensor from $R_{layer\ 2}$ after exposure to SA and dividing by ΔR_{max}. All extinction measurements were collected in a N_2 environment. The solid line is the calculated value of $\Delta R/\Delta R_{max}$ using eqs 4−7. The dashed line is the calculated value of $\Delta R/\Delta R_{max}$ from eq 8.

of an adventitious water layer [92,93] result in λ_{max} variations of ±20 nm. Second, there are significant variations in the structure of these triangular nanoparticles (e.g., in-plane tip retraction) caused by the solvent-annealing step used to remove the adventitious water layer. However, as we have demonstrated previously, samples that have different initial absolute values of λ_{max} have identical sensitivity to the changes in external dielectric environment caused by analyte adsorption.[41] Consequently, it is only the change in the LSPR λ_{max} ($\Delta\lambda_{max}$) that is measured in the experiments reported here. $\Delta\lambda_{max}$ is sample independent and responds only to adsorption of the analyte.

Next, the LSPR λ_{max} shift, $\Delta\lambda_{max} = \Delta R$, versus [SA] response curve was measured over the concentration range 10^{-15} M < [SA] < 10^{-6} M (Figure 5). It should be noted that since the thermodynamic affinity constant corresponding to the binding of SA to surface-confined biotin is so large (vide infra) this interaction is essentially irreversible. Consequently, the LSPR shift measurements reported in Figure 5 are from samples that were incubated in the SA solution for a minimum of 3 h. The LSPR $\Delta R/\Delta R_{max}$ versus [SA] response curve represents only an approximation to an equilibrium measurement. SA, once bound to the surface biotin, cannot be desorbed to return the nanosensor to its initial state. For this reason, each data point in Figure 5 is the result of an independent measurement on a different sample.

Figure 5 shows the experimental data (solid points) plotted as the normalized LSPR λ_{max} shift, $\Delta R/\Delta R_{max}$ versus [SA]. ΔR_{max} is the limiting LSPR response at large [SA]. The experimental $\Delta R/\Delta R_{max}$ versus [SA] response curve can be quantitatively interpreted in terms of a model that makes the following assumptions: (1) there is 1:1 binding of solution-phase multivalent analyte (SA) with different sites but invariant affinities to the surface-bound capture ligand (biotin); (2) the only operative nanoparticle sensing mechanism is the change in the local refractive index caused by the adsorbed analyte (SA); and (3) the measured LSPR λ_{max} shift response, ΔR, is determined only by the thickness, d_{SA}, of the adsorbed analyte layer and its refractive index, n_{SA}.

(93) Hong, S.; Zhu, J.; Mirkin, C. A. *Langmuir* **1999**, *15*, 7897−7900.

The equilibrium surface excess, Γ_{SA} in molecules cm^{-2}, for 1:1 binding of SA to surface-bound biotin is given by the Langmuir isotherm:

$$\Gamma_{SA}/\Gamma_{SA,max} = K_{a,surf}[SA]/(1 + K_{a,surf}[SA]) \qquad (1)$$

where $\Gamma_{SA,max}$ is the saturation value of Γ_{SA} (i.e., the packing density) and $K_{a,surf}$ is the surface-confined thermodynamic affinity constant. Recently, Campbell and co-workers clearly demonstrated that the binding stoichiometry of SA is a function of the surface-bound biotin concentration using SPR spectroscopy.[21] At a surface biotin concentration of 0.34%, 1 SA is bound to 1 surface biotin site, whereas at surface biotin concentrations between 10 and 40% 1 SA is bound to 2 surface biotin sites. The surface biotin concentration in our experiments is not known from direct experimental evidence; however, it can be estimated reliably enough to support the 1:1 SA-to-biotin binding hypothesis. The 3:1 ratio of 1-OT/11-MUA yields a 10% surface coverage of carboxylate sites. The conversion of surface carboxylate sites to surface biotin sites via EDC (1 mM) coupling is only ∼1−5% efficient[92], yielding an estimated surface biotin concentration of 0.1−0.5%. Consequently, the 1:1 binding model is a reasonable approximation.

In a manner analogous to Campbell's treatment for the quantitative interpretation of SPR spectroscopy,[18] the LSPR λ_{max} shift response, R (in nm), is given by

$$R = m(n_{eff} - n_{ext}) \qquad (2)$$

where m is the refractive index sensitivity of the NSL-derived Ag nanoparticles that make up the LSPR nanobiosensor, n_{ext} is the bulk refractive index of the external medium ($n_{ext} = n_{N_2}$ = 1.00 for N_2 in the experiments reported here), and n_{eff} is the effective refractive index of the trilayer structure (viz., layer 1 = 1-OT/11-MUA/biotin, layer 2 = SA, and layer 3 = N_2(g)) above the Ag nanoparticle sensor surface. Previous studies on the effect of the bulk external dielectric medium on the LSPR λ_{max} have verified that eq 2 is valid for triangular Ag nanoparticles (∼100 nm wide and 50 nm high) with no adsorbate overlayer (m = 191 nm RIU^{-1}) and surface-modified with a monolayer of $CH_3(CH_2)_{15}SH$ (m = 150 nm RIU^{-1}).[41,92] The effective refractive index of the trilayer structure is obtained by integrating the distance-dependent local refractive index, $n(z)$, weighted by the square of the local electromagnetic field, $E(z)$, from zero to infinity:[18]

$$n_{eff} = \frac{2}{l_d}\int_0^\infty n(z)E^2(z)\,dz$$

$$n(z) = \begin{cases} n_{SAM} & 0 \le z \le d_{SAM} \\ n_{SA} & d_{SAM} \le z \le d_{SAM} + d_{SA} \\ n_{N_2} & d_{SAM} + d_{SA} \le z \le \infty \end{cases} \qquad (3)$$

$E(z)$ is assumed to be dependent only on the local surface normal, z, and to have a single characteristic decay length, l_d. Although the electromagnetic field distribution surrounding these triangular Ag nanoparticles is known to be considerably more complex,[72] this simplification serves well to illustrate the behavior of the LSPR nanobiosensor. The factor, $2/l_d$, normalizes the integral in eq 3 so that $n_{eff} = n_{ext}$ when $n(z) = n_{ext}$ for all z. Next, the functional form of $E(z)$ needs to be determined. Recent studies on the long-range distance dependence of $E(z)$ involving

the measurement of the LSPR wavelength shift caused by multilayer adsorbates reveal that $E(z)$ is a monotonic, but not exponential, decay with a saturation distance of ~30 nm.[94] To reveal the essential physics of the current situation, we will, nevertheless, assume an exponential form for the decay of the local field, $E(z) = \exp(-z/l_d)$, with $l_d \sim 5-6$ nm consistent with the observed saturation distance of ~30 nm. Equation 3 can now be evaluated explicitly and substituted into eq 2 to give the measured response $\Delta R = R_{\text{layer 2}} - R_{\text{layer 1}}$:[18]

$$\Delta R = m(n_{SA} - n_{N_2})[\exp(-2d_{SAM}/l_d)][1 - \exp(-2d_{SA}/l_d)] \quad (4)$$

where d_{SA} is given by[18]

$$d_{SA}/d_{SA,max} = K_{a,surf}[SA]/(1 + K_{a,surf}[SA]) \quad (5)$$

The thickness of the SAM layer, d_{SAM}, is approximated by the thickness of 1-OT only and is given by[95]

$$d_{SAM} = a_1 x + a_2 \quad (6)$$

where x = number of CH_2 units in 1-OT = 7. The constants $a_1 = 0.13$ nm and $a_2 = 0.66$ nm were determined by ellipsometry.[95] The maximum LSPR response, ΔR_{max}, is

$$\Delta R_{max} = m(n_{SA} - n_{N_2})[\exp(-2d_{SAM}/l_d)][1 - \exp(-2d_{SA,max}/l_d)] \quad (7)$$

The ratios of eqs 4 and 7 gives a predicted normalized LSPR response that may be compared with experiment. Figure 5 shows the comparison of the experimental $\Delta R/\Delta R_{max}$ response (solid points) with the predicted $\Delta R/\Delta R_{max}$ response (solid line) from eqs 4−7 using the following experimentally determined values: $m = 190$ nm RIU^{-1},[41] $n_{SAM} = 1.463$,[18] $n_{N_2} = 1.00$, $n_{SA} = 1.57$,[18] $l_d = 6.0$ nm (vide supra), and $d_{SAM} = 1.57$ nm[95] and two adjustable parameters, $K_{a,surf}$ and $\Gamma_{SA,max}$. The value of $\Gamma_{SA,max} = 1.74 \times 10^{12}$ molecules cm^{-2} was chosen so that the ΔR_{max} calculated from eq 7 using $d_{SA,max} = \Gamma_{SA,max} V_{SA}$ and the molecular volume of SA, $V_{SA} = (4.2 \times 4.2 \times 5.2$ nm$^3)$[43,96] matched the experimentally determined, $\Delta R_{max} = 26.5$ nm. $K_{a,surf}$ was then adjusted to 10^{11} M^{-1} to give the best fit to the experimental data. Two conclusions can be immediately drawn. First, the saturation surface coverage of SA result is quite reasonable given that one monolayer of the1-OT/11-MUA SAM corresponds to ~4.4×10^{13} carboxylate sites cm^{-2}, which are converted by the ~5% efficient EDC coupling reaction to ~2.2×10^{12} surface biotins cm^{-2}. This corresponds approximately to 1 SA/surface biotin. Second, it is noted that $K_{a,surf} = 10^{11}$ M^{-1} corresponds to a smaller surface binding constant between SA and biotin compared to its solution value, $K_a = 10^{13}-10^{15}$ M^{-1}.[97] This is likely a consequence of the length of the biotin tether chosen for these experiments. It is anticipated that, by increasing the tether length, the surface binding constant will approach that for the solution phase.

Figure 5 also shows for comparison the limiting $\Delta R/\Delta R_{max}$ response (dashed line) for the case where $2d_{SA} \ll l_d$, which reduces to the Langmuir adsorption isotherm:

$$\frac{\Delta R}{\Delta R_{max}} = \frac{d_{SA}}{d_{SA,max}} = \frac{\Gamma_{SA}}{\Gamma_{SA,max}} = \frac{K_{a,surf}[SA]}{1 + K_{a,surf}[SA]} \quad (8)$$

Although this approximation is not valid for the SA/biotin/Ag nanobiosensor system discussed here (viz., $d_{SA,max} = 1.6$ nm, $l_d = 6.0$ nm so that $2d_{SA,max}$ is NOT $\ll l_d$), Figure 5 shows that the Langmuir adsorption isotherm is only slightly shifted to higher [SA] compared to the response calculated from eqs 4−7.

In addition, the data in Figure 5 allows one to estimate the limit of detection for the LSPR nanobiosensor. The peak-to-peak wavelength shift noise of the baseline in repetitive experiments is ~0.5 nm. Taking the limit of detection as three times this value, one conservatively estimates a LOD of <1 pM. Since the inherent peak-to-peak wavelength shift noise of the miniature CCD spectrometer is ~0.2 nm and this could be improved further by adding temperature stabilization, we anticipate that, with further improvements in the LSPR nanobiosensor itself, most notably the structural stability of the Ag nanoparticles and their adhesion to the substrate, a LOD in the high-femtomolar range can be achieved. It is important to note that the LOD is also critically dependent on the K_a for the species. The LOD will increase for higher binding affinities and decrease for lower binding affinities.

A further point regarding the LOD should be made. All of the data reported in this paper are derived from macroscopic UV−visible extinction spectroscopy measurements (probe beam diameter, 4 mm) on single-layer NSL nanoparticle arrays. Since the areal density of these samples is 1.5×10^9 nanoparticles cm^{-2}, 1.9×10^8 nanoparticles are interrogated. Assuming that each nanoparticle is a truncated tetrahedron with surface area of 1.4×10^{-10} cm^2 [41,86] and the maximum SA saturation coverage = 1.74×10^{12} molecules cm^{-2} (vide supra), the number of SA molecules per nanoparticle at saturation coverage is ~2.44×10^2. For bulk SA concentrations near the LOD, there might be as few as 2.44×10^1 SA molecules/nanoparticle. Consequently, in our present experiments, the LOD corresponds to 4.6×10^9 SA molecules/sample.

A reasonable extrapolation of these data demonstrates that the LSPR nanobiosensor may have a very bright future in high-throughput screening applications where an important figure of merit for the signal transduction platform is the minimum number of target analyte molecules per sensor element in an array that can be detected. Previously, we demonstrated that the macroscopic UV−visible extinction spectroscopy of a single-layer NSL sample is identical to the corresponding spatially resolved UV−visible microextinction spectroscopy experiment using a probe beam diameter of 12 μm.[92] Thus, it may reasonably be expected that data similar to that shown in Figure 5 could be obtained from a field of view that is 1.1×10^5 times smaller. In this circumstance, the LOD would correspond to only 4.2×10^4 SA molecules for a sensor element containing 1.7×10^3 nanoparticles. This still may not be the ultimate limit. We have shown that single-layer NSL-derived Ag nanoparticles have sufficiently large interparticle spacing that they are weakly or not electromagnetically coupled.[86] Consequently, each nanoparticle functions independently rather than as an array. Thus, the use of recently developed single-nanoparticle spectroscopic techniques[80] is likely to enable the actual detection of ~30 SA

(94) Haes, A. J.; Duyne, R. P., in preparation.
(95) Walczak, M. M.; Chung, C.; Stole, S. M.; Widrig, C. A.; Porter, M. D. *J. Am. Chem. Soc.* **1991**, *113*, 2370−2378.
(96) Connolly, S.; Rao, S. N.; Fitzmaurice, D. *J. Phys. Chem. B* **2000**, *104*, 4765−4776.
(97) Jeppesen, C.; Wong, J. Y.; Kuhl, T. L.; Israelachvili, J. N.; Mullah, N.; Zalipsky, S.; Marques, C. M. *Science* **2001**, *293*, 465−468.

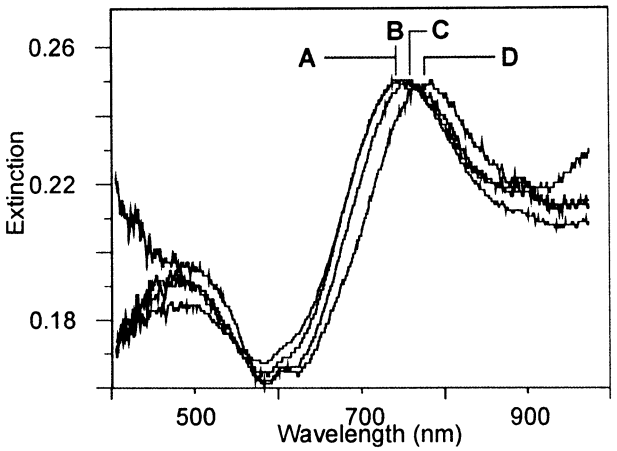

Figure 6. LSPR spectra illustrating the nonspecific binding of SA to a Ag nanobiosensor with no covalently linked biotin. (A) Ag nanoparticles after modification with 1 mM 1:3 11-MUA/1-OT, $\lambda_{max} = 731.5$ nm. (B) Ag nanoparticles after exposure to 100 nM SA, $\lambda_{max} = 732.0$ nm. (C) Ag nanoparticles after modification with 1 mM biotin, $\lambda_{max} = 742.0$ nm. (D) Ag nanoparticles after second exposure to 100 nM SA, $\lambda_{max} = 764.1$ nm. All extinction measurements were collected in a N_2 environment.

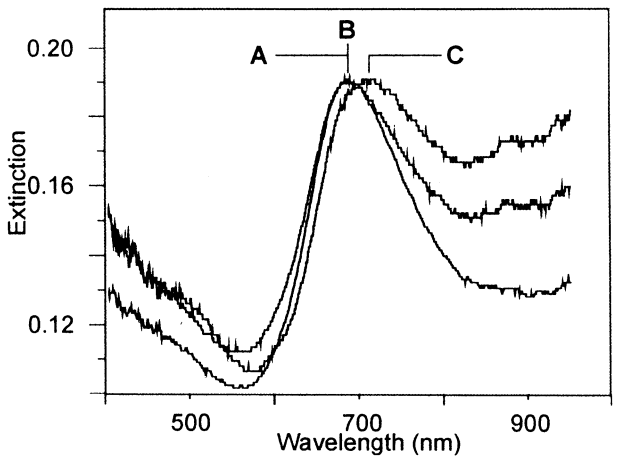

Figure 7. LSPR spectra illustrating the nonspecific binding of prebiotinylated SA to a biotinylated Ag nanobiosensor. All extinction measurements were collected in a N_2 environment. (A) Ag nanoparticles after modification with 1 mM biotin, $\lambda_{max} = 685.4$ nm. (B) Ag nanoparticles after exposure to 100 nM SA that was preexposed to 4 equiv of biotin, $\lambda_{max} = 684.1$ nm. (C) Ag nanoparticles after modification with 100 nM SA, $\lambda_{max} = 709.5$ nm.

molecules by the LSPR nanobiosensor approach presented here. Future improvements in these size and shape tunable LSPR nanosensor materials coupled to the amplification of the LSPR wavelength shift from gold colloid "sandwich" assays may, one day, enable LSPR nanobiosensors to reach sensitivities of a few molecules, perhaps even a single molecule, per sensor element.

Nonspecific Binding Studies. The extraordinary sensitivity of the LSPR nanobiosensor notwithstanding, its practical LOD will be determined by the nonspecific interactions between the capture ligands on the sensor surface and interfering analytes in the sample. To verify that the LSPR nanobiosensor response reported in Figure 5 is the result of specific binding between SA and the biotinylated surface, three nonspecific binding tests were performed: (1) SA interacting with a sensor surface containing no covalently linked biotin; (2) prebiotinylated SA interacting with a biotinylated sensor surface; and (3) BSA interacting with a biotinylated sensor surface.

(1) SA Interacting with a Sensor Surface Containing No Covalently Linked Biotin. First, the Ag LSPR nanobiosensor surface was functionalized with a mixed SAM yielding $\lambda_{max} = 731.5$ nm (Figure 6A). Next, the nanobiosensor surface was exposed to 100 nM SA and thoroughly rinsed, yielding $\lambda_{max} = 732.0$ nm (Figure 6B). The measured LSPR shift is +0.5 nm, a value on the order of the peak-to-peak wavelength shift noise in the baseline of repetitive experiments. To verify that the nanobiosensor surface remained active, the Ag nanoparticles were functionalized with biotin yielding $\lambda_{max} = 742.0$ nm (Figure 6C) and then exposed to 100 nM SA yielding $\lambda_{max} = 764.1$ nm (Figure 6D). The +22.1 nm LSPR shift clearly indicates that the nanobiosensor surface remained active although a ~16% loss of sensing activity was observed in this experiment.

(2) Prebiotinylated SA Interacting with a Biotinylated Sensor Surface. By exposing a biotinylated Ag nanoparticle surface to a 100 nM SA solution in which its binding sites were blocked with four biotin molecules, a second nonspecific interaction test was performed (Figure 7). The biotinylated surface ($\lambda_{max} = 685.4$ nm, Figure 7A) was exposed to the prebiotinylated SA solution for 3 h, yielding $\lambda_{max} = 684.1$ nm (Figure 7B) corresponding to a small LSPR blue-shift of −1.3 nm. Upon exposure to 100 nM SA, the LSPR nanobiosensor once again displayed normal biosensing activity with a LSPR red-shift of +25.0 nm (Figure 7C) that is 94% of ΔR_{max}.

(3) BSA Interacting with a Biotinylated Sensor Surface. To test nonspecific (viz., electrostatic) protein interactions with the biotinylated LSPR nanobiosensor surface and to simulate the effect of a large serum protein background in a clinical sample, BSA interactions with the Ag nanoparticle surface were tested (Figure 8). For this study, the biotinylated nanobiosensor surface ($\lambda_{max} = 707.1$ nm, Figure 8A) was exposed to 1 mg/mL BSA yielding $\lambda_{max} = 709.1$ nm (Figure 8B) corresponding to a small LSPR red-shift of +2.0 nm due to the nonspecific binding. To demonstrate that LSPR nanobiosensor activity was retained following BSA exposure, the surface was exposed to 100 nM SA yielding $\lambda_{max} = 733.6$ nm (Figure 8C) corresponding to a LSPR red-shift of +26.5 nm that is 100% of ΔR_{max}.

Specific Interaction of Anti-Biotin with a Biotinylated Sensor Surface. Anti-biotin should also exhibit specific binding to a biotinylated LSPR nanobiosensor surface. Anti-biotin binds to biotin with a smaller affinity constant ($K_a \sim 2 \times 10^8$ M^{-1} [98]) than SA and has a molecular mass (150 kDa) 2.5 times larger than SA (60 kDa). Since the LSPR nanobiosensor response is determined by the adsorbate-induced local refractive index change, which in turn is directly related to the optical thickness of the target analyte at saturation coverage, we anticipate that anti-biotin should result in a larger LSPR shift than SA. This expectation is confirmed by the results show in Figure 9. The biotinylated nanobiosensor surface ($\lambda_{max} = 686.8$ nm, Figure 9A) was exposed to 0.1 mg/mL anti-biotin yielding $\lambda_{max} = 726.5$ nm (Figure 9B) corresponding to a large LSPR red-shift of +39.7 nm due to the specific binding. This shift is much larger than the $\Delta R_{max} = +26.5$ nm response from SA binding at saturation coverage. Finally, we demonstrate that the LSPR nanobiosensor no longer responds to SA when it is saturated with anti-biotin (Figure 9C). The anti-biotin saturated nanosensor surface was exposed to 100 nM SA, yielding $\lambda_{max} = 726.2$ nm,

(98) Adamczyk, M.; Mattingly, P. G.; Shreder, K.; Yu, Z. *Bioconjugate Chem.* **1999**, *10*, 1032−1037.

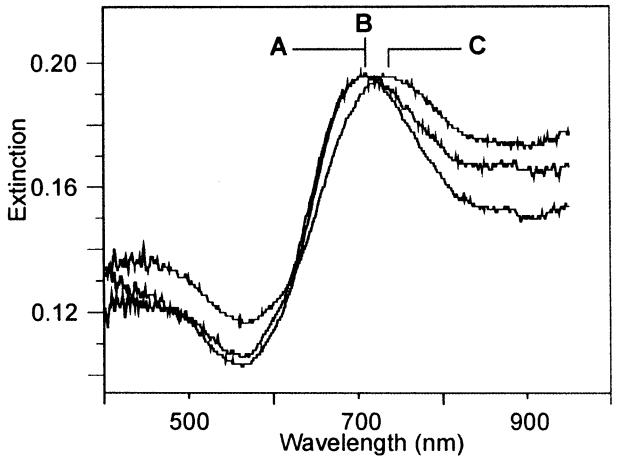

Figure 8. LSPR spectra illustrating the nonspecific binding of BSA to a biotinylated Ag nanobiosensor. All extinction measurements were collected in a N_2 environment. (A) Ag nanoparticles after modification with 1 mM biotin, $\lambda_{max} = 707.1$ nm. (B) Ag nanoparticles after exposure to 1 mg/mL BSA, $\lambda_{max} = 709.1$ nm. (C) Ag nanoparticles after exposure to 100 nM SA, $\lambda_{max} = 733.6$ nm.

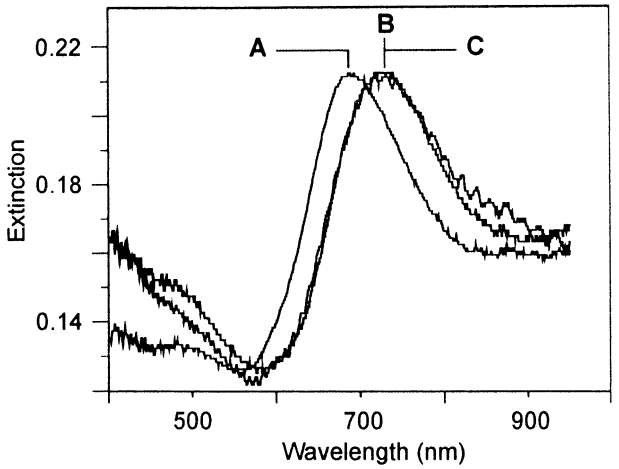

Figure 9. LSPR spectra illustrating the specific binding of anti-biotin to a biotinylated Ag nanobiosensor. All extinction measurements were collected in a N_2 environment. (A) Ag nanoparticles after modification with 1 mM biotin, $\lambda_{max} = 686.8$ nm. (B) Ag nanoparticles after modification with 0.1 mg/mL anti-biotin, $\lambda_{max} = 726.5$ nm. (C) Ag nanoparticles after exposure to 100 nM SA, $\lambda_{max} = 726.2$ nm.

which corresponds to small LSPR blue-shift of -0.3 nm, indicating that all biotin surface sites are bound to anti-biotin.

Conclusions

The principal discovery reported herein is that triangular silver nanoparticles fabricated by nanosphere lithography do indeed function as unexpectedly sensitive and selective nanoscale affinity biosensors. LSPR nanosensors possess at least two unique characteristics that can be tuned by changing nanoparticle size and shape: (1) modest refractive sensitivity on the order of 1 part in 10^2 and (2) a short-range, sensing length scale determined by the characteristic decay length of the local electromagnetic field. These two factors combine to yield an areal mass sensitivity of $\sim 100-1000$ pg/mm^2, which is only a factor of 100 poorer than the best propagating SPR sensitivities. LSPR nanosensors retain all of the other desirable features of SPR spectroscopy.

These important results were unequivocally established through five lines of investigation. First, it was demonstrated that LSPR spectroscopy could be used to monitor all of the steps in the fabrication and surface functionalization of the nanobiosensor. Exposure of the fully functionalized nanosensor to 100 nM SA produced a $+27.0$ nm red-shift in the LSPR spectrum. Similarly, exposure to 1 pM SA produced a small, but measurable, response of $+4.0$ nm. Second, a method was discovered to amplify the LSPR nanobiosensor response. The $+27$ nm LSPR wavelength shift produced by 100 nM SA was amplified by 300% to produce a total LSPR wavelength shift of $+83$ nm by using biotinylated Au colloids in a variation of the classic "sandwich" bioassay. We anticipate that substantial improvements in the LOD can be achieved using this amplification technique. Third, the LSPR λ_{max} shift, ΔR, versus [SA] response curve was measured over the concentration range 10^{-15} M $<$ [SA] $< 10^{-6}$ M. It was found that this response could be interpreted quantitatively in terms of a model involving (1) 1:1 binding of a ligand to a multivalent receptor with different sites but invariant affinities and (2) the assumption that only adsorbate-induced local refractive index changes were responsible for the operation of the LSPR nanosensor. This model yielded values for the saturation response, $\Delta R_{max} = +26.5$ nm, surface-confined thermodynamic binding constant $K_{a,surf} = 10^{11}$ M^{-1}, and LOD $<$ 1 pM. Fourth, a set of control experiments were performed to show that SA binding to a sensor surface containing no biotin, prebiotinylated SA binding to a sensor surface with biotin, and BSA in large excess, simulating a clinical sample, binding to a sensor surface with biotin all produce wavelength shift responses less than that corresponding to the LOD. Finally, it was shown that the LSPR response qualitatively scales with analyte molecular weight by studying the specific binding of anti-biotin to a biotinylated sensor surface. We conclude that the LSPR nanobiosensor is extraordinarily sensitive and selective.

Briefly looking to the future, a reasonable extrapolation of our current data leads us to expect that by optimizing these size and shape tunable nanosensor materials, amplifying the LSPR wavelength shift using the gold (or silver) colloid "sandwich" technique, and using single-nanoparticle spectroscopic techniques, it will be possible to do the following: (1) reach sensitivities of a few molecules, perhaps even a single molecule, per nanoparticle sensor element; (2) reduce the time scale for real-time detection and the study of protein binding kinetics by $2-3$ orders of magnitude since nanoparticle sensor elements will operate in radial rather than planar diffusion mass transport regime; and (3) implement massively parallel bioassays for high-throughput screening applications while maintaining extremely low sample volume requirements. Finally, we point out that LSPR nanosensors can be implemented using extremely simple, small, light, robust, low-cost equipment for unpolarized, UV$-$visible extinction spectroscopy in transmission or reflection geometry. The instrumental simplicity of the LSPR nanosensor approach is expected to greatly facilitate field-portable environmental or point-of-service medical diagnostic applications.

Acknowledgment. The authors gratefully acknowledge financial support from the Army Research Office MURI Program (DAAG-55-97-0133), the National Science Foundation (DMR-0076097 and EEC-0118025), and The Proctor and Gamble Co. (University Exploratory Research Program).

JA020393X